Analytical Dynamic Analysis under Impulse Loadings Using Laplace Transform

Jalal Akbari*

Associate Professor, Department of Civil Engineering, Bu-Ali Sina University, Hamedan, Iran
 j.akbari@basu.ac.ir, https://orcid.org/0000-0001-9713-8652

Samaneh Mirzaei

University of Genoa, Savona compose, Genoa, Italy, 5061574@studenti.unige.it

The application of impulse loading is commonly observed in practice, and accurately estimating the corresponding response through numerical techniques poses significant challenges. This study introduces an analytical formulation to assess the dynamic responses of multi-degree-of-freedom (MDF) beams subjected to impact loading, utilizing the Laplace transform. By focusing on simple beam configurations, this research aims to illuminate previously unexplored aspects of the system's dynamic behavior under impulse loading. Throughout the investigation, any arbitrary or irregular impact loading in the time domain was transformed into the Heaviside step function using the Laplace transform technique. Initially, analytical forced-vibration responses corresponding to the impact loading were mathematically derived. Subsequently, the proposed forced-vibration formulation was validated through laboratory-scale experimental tests. The experimental data were also used to update the finite element model (FEM) for evaluating numerical responses using the Newmark HHT-alpha method under short-time loading. The results indicate that unconditionally stable schemes, such as Newmark HHT-alpha, encounter challenges related to numerical damping, amplitude decay, period elongation, and spurious frequency errors when subjected to impulse loading; however, the proposed method effectively mitigates these errors. The robustness of the proposed method was examined for unusual shock-type loads, and the results demonstrate that the error associated with traditional methods, such as the Newark HHT method is significantly high, with some cases exceeding 300 %.

1. Introduction

Accurately estimating dynamic responses is a critical task across various engineering disciplines. Typically, numerical techniques are employed to assess vibration responses, with the finite element method (FEM) serving as a suitable tool for this purpose. It is essential to minimize modeling errors, which may arise from factors such as finite element mesh size, idealization, material properties, and inaccuracies in boundary conditions. Consequently, numerical model updating is an effective technique for obtaining reliable responses. This approach integrates the structural responses derived from FEM with the measured structural responses to refine the mathematical model. For estimating dynamic responses, the Newmark and HHT-alpha methods demonstrate commendable performance under regular loading, such as harmonic and earthquake excitations. However, the

Newmark average acceleration and HHT-alpha methods are inherently unconditionally stable and may not accurately estimate structural responses under short-duration or impact loadings; therefore, alternative methods should be considered.

Many researchers have investigated the transient responses of structural systems subjected to impact loading. For instance, Tagarielli et al. assessed the vibration responses of composite sandwich beams under shock loading conditions [1] . Wan et al. evaluated the dynamic responses of clamped sandwich beams under impulse loading using both experimental and numerical methodologies [2]. Mazurkiewicz et al. correlated numerical results with experimental data for structural members subjected to impact loading[3]. Zhang et al. conducted an experimental study to evaluate the dynamic response of laminated glass under impulsive and blast loading[4]. Mohammad et al. presented an analytical model for a pipe subjected to an impulse load [5]. Stoynova and Christov estimated the transient responses of reinforced concrete (RC) beams under impact loads[6]. Børvik et al. provided finite element analyses of structural responses to planar blast loads [7]. Shiuh-Chuan and Ching-Chun proposed a model for the elastic responses of a composite shell structure subjected to impact loading[8].

Model updating methodologies are typically categorized into Frequency Response Function (FRF)-based methods. Modal-based techniques rely on the characteristics of modal data obtained from experimental modal analysis. In contrast, FRF-based techniques identify unknown structural parameters by utilizing measured FRF information. Generally, the objective of the FRF-based model updating technique is to minimize the discrepancy between experimental and analytical input forces and output responses. Numerous researchers have employed vibration data for finite element model updating. For instance, Pradhan and Modak introduced a normal FRF approach to update the stiffness and mass matrices of structures[9]. Several studies have focused on updating damped models. Arora et al. and Yuan and Yu applied the FRF method to update finite element models in damped scenarios using vibration data [10, 11]. Yuan utilized vibration data subjected to base excitation to update an undamped system [12]. Additionally, Garcia and Santini implemented a model-updating scheme for updating damped structural systems [13].

From an analytical perspective, several investigations have focused on model-updating techniques. Esfandiari et al.[14, 15], Sipple and Sanayei applied numerical techniques for model updating[16]. Li and Hong [17], and as well Weng et.al [18] implemented model reduction and an iterative approach to enhance the numerical model. Papadimitriou and Papdioti employed the mode synthesis technique for finite element (FE) model updating[19]. The minimum least-squares residual method for model updating was employed by Sarmadi et al. [20]and Wei et al. implemented the intrinsic chirp component decomposition method to update multi-degree-of-freedom systems [21]. Furthermore, the incorporation of optimization methods in model-updating techniques is noteworthy. Christodoulou et al. [22] utilized a Pareto optimization approach for model updating, while Jung and Kim implemented a hybrid genetic algorithm for finite-element model updating [23].

Additionally, Shabbir and Omenzetter applied the particle swarm optimization method for dynamic finite element model updating [24].

To the best of the authors' knowledge, the transient responses of MDF systems utilizing the Newmark HHT-alpha techniques under impact loads are unreliable when finite element modeling is employed [25]. Consequently, alternative methods should be adopted to accurately assess the dynamic responses to such loads. In light of this, the authors propose an analytical method to achieve this objective.

For the forced vibration response, the beam was excited using a hammer. Due to the irregular nature of the hammer load, an analytical Heaviside loading function is proposed in the time domain to replace instead of any arbitrary and irregular loadings.

Then, a numerical model of the beam was developed using finite element methods (FEM), from which modal data were extracted based on frequency response functions (FRF). The numerical model was then updated using the particle swarm optimization (PSO) technique. After the update, the numerical responses of the beam subjected to impulse loading were computed using the Newmark HHT-alpha schemes, and the results were compared with experimental tests. The numerical results indicate that the Newmark HHT-alpha method faces challenges related to numerical damping, amplitude decay, period elongation, and spurious frequency errors when subjected to impulse loading. Ultimately, the beam responses to the hammer load were calculated analytically by employing the proposed method, and the results were again compared with experimental data to validate the proposed approach.

2. Problem description

This section presents analytical free and forced vibration responses of an aluminum beam subjected to impulse loadings. Here, the forced vibration response, $Z(t)$, in the time domain is transformed to $Z(s)$ using the Laplace transform and then reverted to the time domain through the application of the inverse Laplace transform. Ultimately, the beam's responses to impact loading are calculated analytically by employing the superposition principle on the separated responses.

2-1. Free vibration response

The modal information in the analysis of free vibration, including natural frequencies and mode shapes, was determined by solving the differential equation associated with the beam under investigation. The study focused on a cantilever beam with a rectangular cross-section, a length denoted as L, and a mass M located at its free end. (Figure 1)
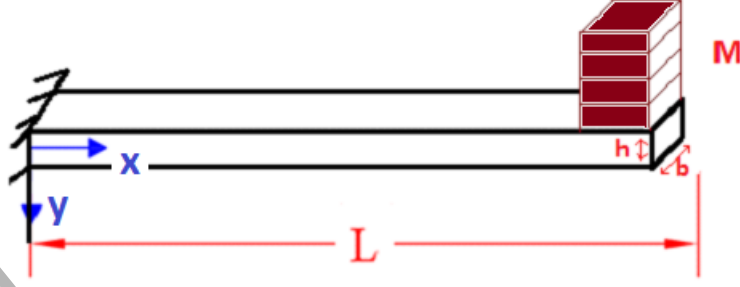
Fig.1 Analytical model of the present study

The forced vibration equilibrium equation of the Euler-Bernoulli beams is obtained as Eq.(1)

$$EI\frac{\partial^4 y(x,t)}{\partial x^4} + \rho A \frac{\partial^2 y(x,t)}{\partial t^2} = p(x,t) \tag{1}$$

In Eq. (1), ρA denotes the mass per unit length, while p(x, t) represents the applied load on the structure. The variable y (x, t) indicates the displacement in the y-direction. In the free-vibration analysis, the right-hand side of Eq.(1) is zero. Consequently, Eq. (1) for free vibration is expressed as Eq.(2).

$$a^2 \frac{\partial^4 y(x,t)}{\partial x^4} + \frac{\partial^2 y(x,t)}{\partial t^2} = 0 \quad ; \quad a = \sqrt{\frac{EI}{\rho A}} \tag{2}$$

The separation variable method is employed to solve Eq.(2), is expressed as Eq.(3)

$$y(x,t) = \phi(x)z(t)$$
$$a^2 \phi^{IV}(x)z(t) + \phi(x)\ddot{z}(t) = 0 \tag{3}$$

The free vibration equation denoted as Eq. (2), is rewritten into two distinct equations as Eq. (4). One equation is expressed in the time domain as z(t), while the other is represented in the space domain as $\phi(x)$

$$\ddot{z}(t) + \omega^2 z(t) = 0$$
$$\phi^{IV}(x) - \beta^4 \phi(x) = 0 \tag{4}$$

The new parameters are defined as Eq.(5)

$$-a^2 \frac{\phi^{IV}(x)}{\phi(x)} = \frac{\ddot{z}(t)}{z(t)} = -\omega^2 \quad , \quad \beta^4 = \frac{\omega^2}{a^2} \tag{5}$$

The responses of equations (4) are available as Eq.(6).

$$\left.\begin{array}{l} z(t) = A\cos(\omega t) + B\sin(\omega t) \\ \phi(x) = G_1 \cos(\beta x) + G_2 \sin(\beta x) + G_3 \cosh(\beta x) + G_4 \sinh(\beta x) \end{array}\right\} \to y(x,t) = \phi(x)z(t) \tag{6}$$

Here, $z(t)$ is the time domain response, and $\phi(x)$ refers to the mode shape of the beam. The coefficients G_i were derived from the boundary conditions and A, B were determined based on the initial conditions of the

model. As illustrated in Figure 1, both deflection and slope are zero at the supports of the beam. Consequently, Eq.(7) can be expressed as follows:

$$\left.\begin{array}{l} y\left(0,t\right)=0 \\ \dfrac{\partial y}{\partial x}\left(0,t\right)=0 \end{array}\right\} \rightarrow \begin{cases} G_1 + G_3 = 0 \\ G_2 + G_4 = 0 \end{cases} \tag{7}$$

Based on Eq.(7), the mode shape, Eq.(8), is rewritten as follows:

$$\phi\left(x\right)=G_1\left(\cos\left(\beta x\right)-\cosh\left(\beta x\right)\right)+G_2\left(\sin\left(\beta x\right)-\sinh\left(\beta x\right)\right) \tag{8}$$

The boundary conditions of the cantilever beam with a concentrated mass M at the free end are written as Eq.(9).

$$\left.\begin{array}{l} M\left(l,t\right)=0 \\ \dfrac{\partial}{\partial x}\left[EI\dfrac{\partial^2 y\left(l,t\right)}{\partial x^2}\right]=M\left[\dfrac{\partial^2 y\left(l,t\right)}{\partial t^2}\right] \end{array}\right\} \rightarrow \begin{cases} EIy''\left(l,t\right)=0 \\ EIy'''\left(l,t\right)-M\ddot{y}\left(l,t\right)=0 \end{cases} \tag{9}$$

By substituting Eq. (9) into Eq.(8), equations (10) through (12) are derived.

$$G_1\left(\cos\left(\beta l\right)-\cosh\left(\beta l\right)\right)+G_2\left(\sin\left(\beta l\right)-\sinh\left(\beta l\right)\right)=0 \tag{10}$$

$$\frac{EI}{M}\phi'''\left(l\right)=\phi\left(l\right)\frac{\ddot{z}\left(t\right)}{z\left(t\right)}\rightarrow -\frac{EI}{M\omega^2}\phi'''(l)=\phi\left(l\right) \tag{11}$$

$$\frac{EI\beta^3}{M\omega^2}\Big[-G_1\left(\sin\left(\beta l\right)+\sinh\left(\beta l\right)\right)+G_2\left(\cos\left(\beta l\right)+\cosh\left(\beta l\right)\right)\Big]= \tag{12}$$
$$G_1\left(\cos\left(\beta l\right)-\cosh\left(\beta l\right)\right)+G_2\left(\sin\left(\beta l\right)-\sinh\left(\beta l\right)\right)$$

The parameters $\lambda=\beta l$ $\alpha=\bar{m}l/M\lambda$ $\beta^4/\omega^2=EI/\bar{m}$ are substituted into equations (10) and (12), and Eq.(13) can be obtained.

$$\begin{bmatrix} \cos\lambda+\cosh\lambda & \sin\lambda+\sinh\lambda \\ \alpha\left(-\sin\lambda+\sinh\lambda\right)-\cos\lambda+\cosh\lambda & \alpha\left(\cos\lambda+\cosh\lambda\right)-\sin\lambda+\sinh\lambda \end{bmatrix}\begin{bmatrix} G_1 \\ G_2 \end{bmatrix}=\begin{bmatrix} 0 \\ 0 \end{bmatrix} \tag{13}$$

The eigenvalues (λ) of the system are determined when the determinant of Eq.(13) is set to zero, as expressed in Eq.(14).

$$\alpha\left(\cos\lambda+\cosh\lambda\right)^2+\left(\cos\lambda+\cosh\lambda\right)\left(-\sin\lambda+\sinh\lambda\right)+ \tag{14}$$
$$\alpha\left(\sinh^2\lambda-\sin^2\lambda\right)+\left(\sin\lambda+\sinh\lambda\right)\left(-\cos\lambda+\cosh\lambda\right)=0$$

Equation (15) represents the simplified form of Eq.(14). The eigenvalues (λ_n) of the beams were determined by solving the nonlinear Equation (15). To obtain all roots of this nonlinear equation, a specialized numerical solution technique was employed [26].

$$\frac{\left(\sin \lambda_n \cosh \lambda_n - \cos \lambda_n \sinh \lambda_n\right)}{1 + \cos \lambda_n \cosh \lambda_n} - \frac{\bar{m}l}{M \lambda_n} = 0 \tag{15}$$

The frequencies of vibration (ω_n) in each mode are determined according to Eq.(16).

$$\lambda_n^{2} = \omega_n l^{2} \sqrt{\frac{\bar{m}}{EI}} \rightarrow \omega_n = (\frac{\lambda_n}{l})^{2}\sqrt{\frac{EI}{\bar{m}}} \tag{16}$$

The values of coefficients G_1, G_2 must be known to determine the mode shapes corresponding to each vibration mode. Here, G_1 is set to 1.0, and the general values G_n are derived from Eq.(17)

$$G_n = \frac{\alpha_n \cos \lambda_n + \alpha_n \cosh \lambda_n - \sin \lambda_n + \sinh \lambda_n}{\alpha_n \sin \lambda_n - \alpha_n \sinh \lambda_n + \cos \lambda_n - \cosh \lambda_n}$$
$$\lambda_n = \beta_n l \ : \ \alpha_n = \frac{\bar{m}l}{M \lambda_n} = \frac{\bar{m}}{\beta_n M} \tag{17}$$

Finally, the mode shapes for the beam are obtained according to Eq.(18)

$$\phi_n \left(x\right) = \sin \beta_n x - \sinh \beta_n x + G_n \left(\cos \beta_n x - \cosh \beta_n x \right)$$
$$\phi_n \left(x\right) = \sin\left(\frac{\lambda_n x}{l}\right) - \sinh\left(\frac{\lambda_n x}{l}\right) + G_n \left(\cos\left(\frac{\lambda_n x}{l}\right) - \cosh\left(\frac{\lambda_n x}{l}\right)\right) \tag{18}$$

2-2. The proposed method for force vibration responses

In this section, analytical formulations of forced vibration responses of the studied beam are derived based on the Laplace transform technique under impulse loadings. For this purpose, the equation of motion under arbitrary loading as Eq.(19) is considered.

$$EI \frac{\partial^4 y \left(x,t\right)}{\partial x^4} + \rho A \frac{\partial^2 y \left(x,t\right)}{\partial t^2} = p\left(t\right) \tag{19}$$

The method of separation of variables is employed once more to solve the equilibrium equation presented in Eq. (19), by Eq.(20)

$$y(x,t) = \sum_{n=1}^{\infty} \phi_n(x) z_n(t) \tag{20}$$

The mode shapes corresponding to the n-th vibration mode, $\phi_n(x)$, are provided by Eq.(18); however, $z_n(t)$ are unknown. By substituting Eq.(20) into Eq.(19), one can derive Eq.(21).

$$\rho A \sum_{n=1}^{\infty} \ddot{z}_n(t)\phi_n(x) + \sum_{n=1}^{\infty} EI\beta_n^{4} z_n(t)\phi_n(x) = p(t) \tag{21}$$

By introducing new variables, such as $\lambda_n = l\beta_n$, $\beta_n^2 = \omega_n \sqrt{\dfrac{\overline{m}}{EI}}$ Eq.(21) is re-written as Eq.(22)

$$\sum_{n=1}^{\infty} \left[EI\beta_n^4 z_n(t) + \rho A\ddot{z}_n(t) \right] \phi_n(x) = p(t) \tag{22}$$

Both sides of Eq.(22) are multiplied by $\displaystyle\int_0^l \phi_m(x)dx$ and Eq.(23) can be obtained.

$$\sum_{n=1}^{\infty} \left[\ddot{z}_n(t) + \frac{EI}{\rho A}\beta_n^4 z_n(t) \right] \times \int_0^l \phi_n(x)\phi_m(x)\,dx = p(t)\int_0^l \phi_m(x)dx \tag{23}$$

The eigenvalues $\phi_m(x)$ $\phi_n(x)$ are expressed as Eqs. (24).

$$\phi_m(x) = \sin\beta_m x - \sinh\beta_m x + G_m\left(\cos\beta_m x - \cosh\beta_m x\right)$$
$$\phi_n(x) = \sin\beta_n x - \sinh\beta_n x + G_n\left(\cos\beta_n x - \cosh\beta_n x\right) \tag{24}$$

By introducing $I_n = \displaystyle\int_0^l \phi_n(x)\phi_m(x)dx$, $J_n = \displaystyle\int_0^l \phi_n(x)dx$ Eq.(23) is rewritten as Eq.(25)

$$\sum_{n=1}^{\infty} \left[\ddot{z}_n(t) + \frac{EI}{\rho A}\beta_n^4 z_n(t) \right] I_n = p(t)J_n \tag{25}$$

Integration $I_n = \displaystyle\int_0^l \phi_n(x)\phi_m(x)dx$ could be rewritten as Eq.(26)

$$
\begin{aligned}
I_n = \int_0^l \phi_n(x)\phi_m(x)\,dx &= \int_0^l \left(\sin\beta_n x \sin\beta_m x\right) - \int_0^l \left(\sin\beta_n x \sinh\beta_m x\right) + \\
&\int_0^l \left(G_m \sin\beta_n x \cos\beta_m x\right) - \int_0^l \left(G_m \sin\beta_n x \cosh\beta_m x\right) - \int_0^l \left(\sinh\beta_n x \sin\beta_m x\right) + \\
&\int_0^l \left(\sinh\beta_n x \sinh\beta_m x\right) - \int_0^l \left(G_m \sinh\beta_n x \cos\beta_m x\right) + \int_0^l \left(G_m \sinh\beta_n x \cosh\beta_m x\right) + \\
&\int_0^l \left(G_n \cos\beta_n x \sin\beta_m x\right) - \int_0^l \left(G_n \cos\beta_n x \sinh\beta_m x\right) + \int_0^l \left(G_n G_m \cos\beta_n x \cos\beta_m x\right) - \\
&\int_0^l \left(G_n G_m \cos\beta_n x \cosh\beta_m x\right) - \int_0^l \left(G_n \cosh\beta_n x \sin\beta_m x\right) + \int_0^l \left(G_n \cosh\beta_n x \sinh\beta_m x\right) - \\
&\int_0^l \left(G_n G_m \cosh\beta_n x \cos\beta_m x\right) + \int_0^l \left(G_n G_m \cosh\beta_n x \cosh\beta_m x\right)
\end{aligned}
\tag{26}
$$

The above integrations are analytically calculated, and the final form I_n is expressed as Eq.(27).

$$I_n = I_1 - 2I_2 + 2G_n I_3 - 2G_n I_4 + I_5 - 2G_n I_6 + 2G_n I_7 + G_n^2 I_8 - 2G_n^2 I_9 + G_n^2 I_{10} \tag{27}$$

The I_i values are determined according to Eq.(28)

$$I_1 = \frac{l}{2} - \frac{\sin 2\beta_n l}{4\beta n} \;;\; I_2 = \frac{\cosh \beta_n l \;\sin \beta_n l - \sinh \beta_n l \;\cos \beta_n l}{2\beta_n} \;;\; I_3 = \frac{1 - \cos 2\beta_n l}{4\beta_n}$$

$$I_4 = \frac{(\sinh \beta_n l \;\sin \beta_n l - \cosh \beta_n l \;\cos \beta_n l) + 1}{2\beta_n} \;;\; I_5 = \frac{\sinh 2\beta_n l}{4\beta_n} - \frac{1}{2}$$

$$I_6 = \frac{(\cosh \beta_n l \;\cos \beta_n l + \sinh \beta_n l \;\sin \beta_n l) - 1}{2\beta_n} \;;\; I_7 = \frac{\cos \beta_n l - 1}{4\beta_n}$$

$$I_8 = \frac{l}{2} + \frac{\sinh 2\beta_n l}{4\beta_n} \;;\; I_9 = \frac{\sinh \beta_n l \;\cos \beta_n l + \cosh \beta_n l \;\sin \beta_n l}{2\beta_n} \;;\; I_{10} = \frac{l}{2} + \frac{\sinh 2\beta_n l}{4\beta_n}$$

(28)

Evaluation $J_n = \int_0^l \phi_n(x)\,dx$ is obtained by Eq.(29).

$$J_n = \int_0^l \phi_n(x)\,dx = \int_0^l (\sin \beta_n x - \sinh \beta_n x + G_n \cos \beta_n x - G_n \cosh \beta_n x)\,dx$$

(29)

Integration of Eq.(29) leads to Eq.(30)

$$J_n = \frac{1}{\beta_n}(2 - \cos\beta_n l - \cosh\beta_n l + G_n \sin\beta_n l - G_n \sinh\beta_n l)$$

(30)

In this instance, as illustrated in Figure 2 (a), we examine a short-time impact load characterized by an arbitrary shape that does not conform to any mathematical function. This load has been converted into an equivalent Heaviside step function, as depicted in Figure 2 (b) [27].
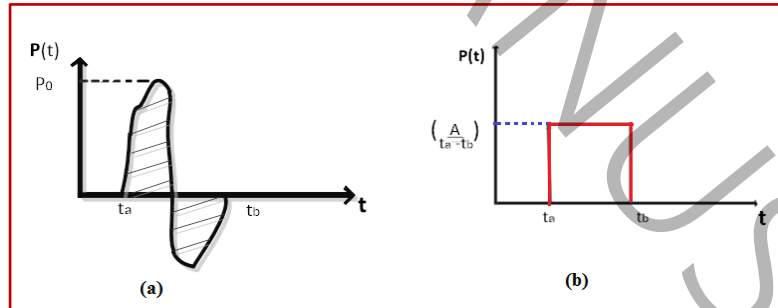

Fig.2- Idealization of arbitrary impulse load (a) into an equivalent step function (b)

The procedure for converting arbitrary impulse loading is as follows: As illustrated in Figure 2 (a), the area (A) under the impulse loading is defined by Eq.(31). In general, numerical integration techniques are employed to calculate this area.

$$A = \int_{t_a}^{t_b} p(t)\,dt$$

(31)

The area under arbitrary impulse loading (A) must be equivalent to the area under a step function loading. Consequently, any arbitrary impact loading can be represented in the form of the Heaviside step function as Eq.(32)

$$p(t) = \frac{A}{t_b - t_a}\left[H\left(t - t_a\right) - H\left(t - t_b\right)\right] = \frac{p_0}{2}\left[H\left(t - t_a\right) - H\left(t - t_b\right)\right] \tag{32}$$

Where $H\left(t - t_a\right), H\left(t - t_b\right)$ are the Heaviside step functions. In addition, t_a, t_b denote the starting and ending points of the impulse loading, respectively. Eq.(25) could be rewritten as Eq.(33) to calculate the responses under impact load.

$$\sum_{n=1}^{\infty}\left[\ddot{z}_n(t) + \omega_n^2 z_n(t)\right] = \frac{J_n}{I_n}p(t) = k_n p(t) \quad ; k_n = \frac{J_n}{I_n} \tag{33}$$

By substituting Eq.(32) into Eq.(33), the time domain response in each mode is determined as Eq.(34)

$$\ddot{z}_n(t) + \omega_n^2 z_n(t) = \frac{p_0 k_n}{2}\left[H\left(t - t_a\right) - H\left(t - t_b\right)\right] \tag{34}$$

The most effective approach for solving Eq.(34) involves the application of the Laplace transform method. Accordingly, the Laplace transform is applied on both sides of Eq.(34), and Eq.(35) can be obtained.

$$L\left[\ddot{z}_n(t) + \omega_n^2 z_n(t)\right] = L\left[0.5 p_0 k_n H\left(t - t_a\right)\right] - L\left[0.5 p_0 k_n H\left(t - t_b\right)\right]$$
$$S^2 z(s) + \omega_n^2 z(s) = 0.5 p_0 k_n\left(\frac{e^{-t_a s}}{s} - \frac{e^{-t_b s}}{s}\right) = \frac{p_0 k_n}{2s}(e^{-t_a s} - e^{-t_b s}) \tag{35}$$

Here, $z(s)$ is the Laplace transform of $z(t)$ and is determined as Eq.(36)

$$Z(s) = \frac{p_0 k_n}{2s(s^2 + \omega_n^2)}(e^{-t_a s} - e^{-t_b s}) \tag{36}$$

The inverse Laplace transform is applied in Eq.(36) to determine the response of the system in the time domain, and Eq.(37) can be obtained by introducing $c_n = p_0 k_n / 2$:

$$L^{-1}\left[\frac{c_n e^{-t_a s}}{s(s^2 + \omega_n^2)}\right] = \frac{c_n H\left(t - t_a\right)}{\omega_n^2}\left[H\left(t - t_a\right) - \cos(\omega(t - t_a))\right] \tag{37}$$

Therefore, the values $z_n(t)$ in the time domain are calculated as Eq.(38)

$$z_n(t) = \left(\frac{c_n H\left(t - t_a\right)}{\omega_n^2}\left[H\left(t - t_a\right) - \cos(\omega_n(t - t_a))\right]\right) - \left(\frac{c_n H\left(t - t_b\right)}{\omega_n^2}\left[H\left(t - t_b\right) - \cos(\omega_n(t - t_b))\right]\right) \tag{38}$$

The response of any system, ($y(x,t)$), under an impact loading at any time and any place finally could be determined by Eq.(39)

$$y(x,t) = \sum_{n=1}^{\infty} \phi_n(x) z_n(t) = (\sin \beta_n x - \sinh \beta_n x + G_n \cos \beta_n x - G_n \cosh \beta_n x) z_n(t) \tag{39}$$

In Eq.(39), the values β_n, G_n are derived from Eq.(17). Furthermore, the acceleration response in the time domain can be obtained from Eq.(40)

$$\ddot{z}_n(t) = \left(\frac{2c_n}{\omega_n^2} \delta(t - t_a) \left[\delta(t - t_a) + \omega_n \sin \omega_n (t - t_a) \right] + c_n H(t - t_a) \cos \omega_n (t - t_a) \right) -$$
$$\left(\frac{2c_n}{\omega_n^2} \delta(t - t_b) \left[\delta(t - t_b) + \omega_n \sin \omega_n (t - t_b) \right] + c_n H(t - t_b) \cos \omega_n (t - t_b) \right) \tag{40}$$

The Dirac delta function at a specified time is represented as t_a is given by $\delta(t - t_a)$. Ultimately, the acceleration response of any system subjected to short-time impact loading, as determined by the proposed method, is expressed in Eq.(41)

$$\ddot{y}(x,t) = \sum_{n=1}^{\infty} \phi_n(x) \ddot{z}_n(t) = (\sin \beta_n x - \sinh \beta_n x + G_n \cos \beta_n x - G_n \cosh \beta_n x) \ddot{z}_n(t) \tag{41}$$

2-3. Modal parameters (numerical results)

The modal parameters, which include frequency, mode shape, and damping ratio, were determined through numerical analysis utilizing the Finite Element Method (FEM). Initially, the aluminum beam was discretized into 25 elements, each with a length of 3 cm. The mass matrix $\mathbf{M}_e$ and stiffness matrix $\mathbf{K}_e$ for each element are presented in Eq.(42).

$$\mathbf{K}_e = \frac{EI}{l^3} \begin{bmatrix} 12 & 61 & -12 & 61 \\ 61 & 41^2 & -61 & 21^2 \\ -12 & -61 & 12 & -61 \\ 61 & 21^2 & -61 & 41^2 \end{bmatrix}; \mathbf{M}_e = \frac{\rho A l}{420} \begin{bmatrix} 156 & 221 & 54 & -131 \\ 221 & 41^2 & 131 & -31^2 \\ 54 & 131 & 156 & -221 \\ -131 & -31^2 & -221 & 41^2 \end{bmatrix} \tag{42}$$

Here, E represents the Young modulus, I denotes the cross-sectional moment of inertia, and l indicates the length of the individual element ($l = L/N_{elem}$). The total length of the beam is denoted as L, which N_{elem} represents the number of elements. Additionally, ρ signifies the mass density of aluminum, and A refers to the cross-section of the beam. A concentrated mass (M) has been affixed to the second node of the last element of the beam. Consequently, this mass must be incorporated into the mass matrix by adding it to the local mass matrix as illustrated in Eq.(43).

$$\mathbf{M}_{con} = \begin{bmatrix} 0 & 0 & 0 & 0 \\ 0 & 0 & 0 & 0 \\ 0 & 0 & M & 0 \\ 0 & 0 & 0 & 0 \end{bmatrix} \qquad (43)$$

2-4. Modal parameters (experimental results)

The aluminum beam was studied experimentally. As presented in Figure 3, the acceleration data was gathered using the hammer force at the specified points. (Unidirectional acceleration sensors at four nodes on the beam are installed).
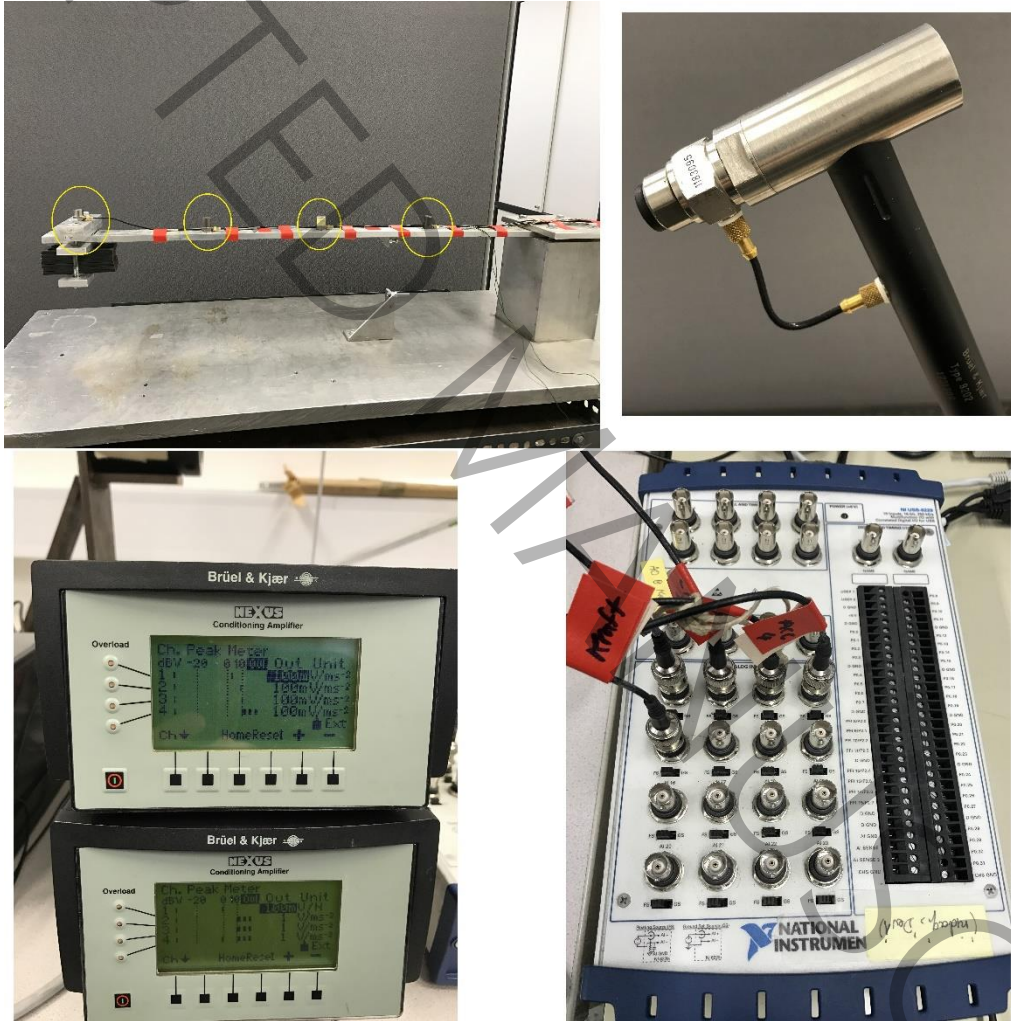

Fig.3-Setup of experimental study including: Beam's geometry, locations of acceleration sensors, hammer and data acquisition system

To collect the experimental data, forces (input data) were recorded at three positions: P1, P2, and P3, while accelerations (output data) were measured at stations CH1, CH2, CH3, and CH4. The duration of the recorded data was 30 seconds, and each test was conducted three times. With a sampling frequency of 400 Hz for the data

acquisition system, a total of 2000 samples were collected for each test over 30 seconds. The necessary experimental modal information was extracted using MATLAB[28].
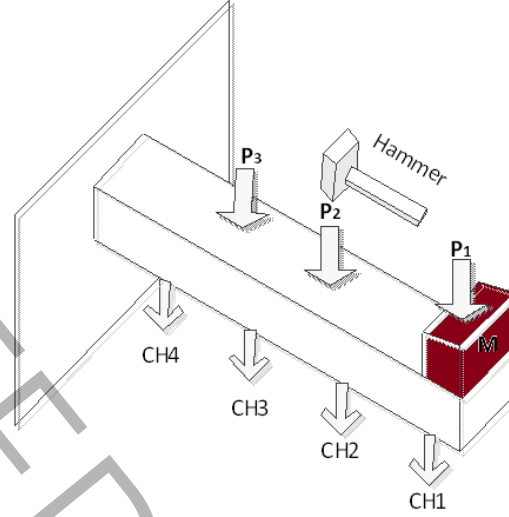

Fig.4 –Positions of P1, P2, and P3 (input forces), and sensors CH1, CH2, CH3, and CH4 (output accelerations)

2-5. Updating the numerical model

In this study, the updating procedure was executed utilizing the Modal Assurance Criterion (MAC) method based on the data collected from the stations specified in the experimental tests, to modify the global stiffness and mass matrices [29]. The updating of the mass and stiffness matrices was carried out employing the Particle Swarm Optimization (PSO) technique [30]. An objective function was formulated using the frequency values and the components of the mode shapes derived from both experimental and numerical data, as presented in Equation (44).

$$f = \sqrt{\left(\left(\omega_i^{num} - \omega_i^{\exp}\right)\Big/\omega_i^{\exp}\right)^2} + \sqrt{\sum_{j=1}^{ndf}\left(\left(\phi_{i,j}^{num} - \phi_{i,j}^{\exp}\right)\Big/\phi_{i,j}^{\exp}\right)^2} \tag{44}$$

Here, $\omega_i^{num}, \phi_{i,j}^{num}$ are the frequencies and jth -components of mode shapes in the FE model, respectively, and $\omega_i^{\exp}, \phi_{i,j}^{\exp}$ are the frequencies and jth-mode shapes of the experimental data, respectively.

3. Results

3-1. Modal parameters

The aluminum beam was studied concerning its geometrical and mechanical properties, as summarized in Table (1).

Table 1- The specifications of the studied beam

ρ(kg/m³)	b(mm)	h(mm)	L(mm)	$\bar{\mathbf{m}}$ (kg/m)	M(kg)	E(GPa)
2700	40	10	750	1.08	1.585	69

The beam was divided into 25 elements, from which the modal parameters were extracted. However, due to the limitations of the measured accelerations in the experimental tests, the finite element (FE) model was subsequently reduced from 25 elements to four elements. The frequency results are detailed in Table 2. The mode shapes of the beam are illustrated through analytical, updated numerical, and experimental tests as shown in Figure 5.

Table 2- Analytical, FE, and experimental values of natural frequencies (rad/s) of the beam

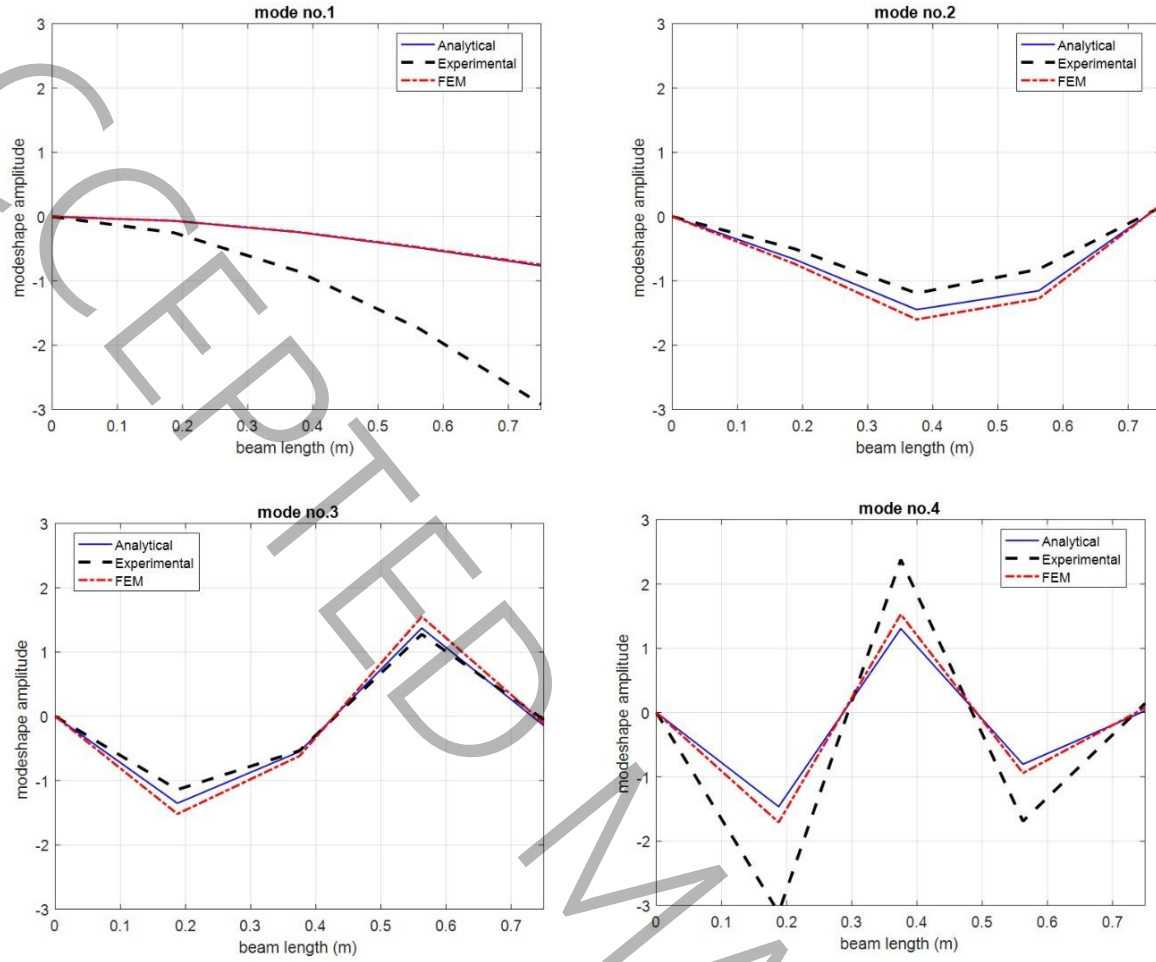| Mode number	Proposed analytical frequencies (Hz)	Numerical frequencies (reduced model) (Hz)	Experimental frequencies (Hz)
1	30.34	30.34	29.34
2	411.78	411.98	341.12
3	1309.29	1317.16	1151.41
4	2715.07	2777.81	2462.11*

Fig.5 –Analytical, numerical (4-element), and experimental mode shapes of the studied beam

As demonstrated in Figure 5, there is a strong correlation among the analytical, finite element (FE), and experimental mode shapes. However, the experimental mode shape observed in the fourth mode exhibits discrepancies when compared to the results obtained from the other methodologies. These differences in the fourth mode may be attributed to the scaling of the mode shapes. The finite element (FE) model was updated to modify the stiffness and mass matrices, utilizing the Particle Swarm Optimization (PSO) algorithm by the proposed objective function outlined in equation (44). The convergence of the objective function is illustrated in Figure 6. Additionally, Table 3 presents the numerical values of the frequencies both before and after the updating process. It is noteworthy that this study focused exclusively on updating numerical models through the use of frequency information.
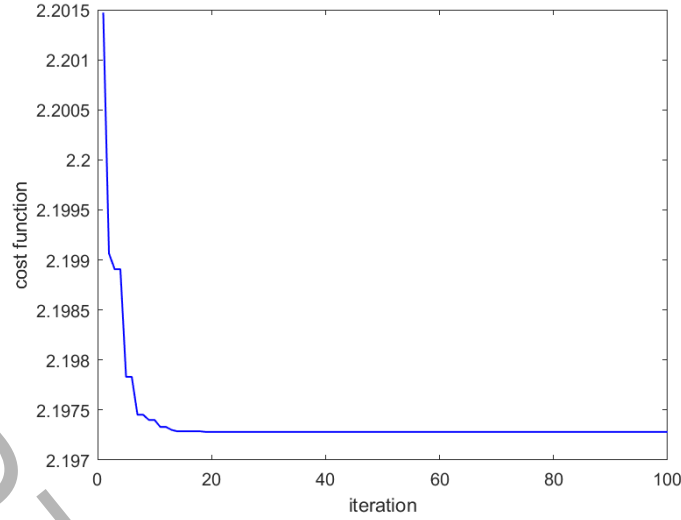
Fig.6- The objective function's convergence of the updating process using the PSO

Table 3- Natural frequencies (rad/s): before and after updating

Mode number	Numerical frequencies (Hz) (before updating)	Numerical frequencies (Hz) (after updating)
1	30.34	28.80
2	411.98	344.83
3	1317.16	1176.92
4	2777.81	2404.61

Table 4 presents the values of the modified mass and stiffness matrices. The automatically updated matrices were used for vibration analysis of the beam under impulse loading.

Table 4- Stiffness and mass matrices of the beam (mass unit is kg and stiffness is N / m)

$$\mathbf{K} = \begin{bmatrix} 702420 & -456600 & 182920 & -33420 \\ -456600 & 546340 & -364610 & 99230 \\ 182920 & -364610 & 366120 & -133460 \\ -33420 & 99230 & -133460 & 5750 \end{bmatrix} \qquad \mathbf{K}^{Update} = \begin{bmatrix} 585230 & -343390 & 131300 & -27830 \\ -343390 & 387810 & -259510 & 74370 \\ 131300 & -259510 & 259630 & -94480 \\ -27830 & 74370 & -94480 & 39910 \end{bmatrix}$$

$$\mathbf{M} = \begin{bmatrix} 0.175 & 0.015 & -0.007 & 0.01 \\ 0.015 & 0.189 & 0.008 & -0.017 \\ -0.007 & 0.008 & 0.196 & 0.035 \\ 0.01 & -0.017 & 0.035 & 1.639 \end{bmatrix} \qquad \mathbf{M}^{Update} = \begin{bmatrix} 0.182 & 0.014 & -0.01 & 0.011 \\ 0.014 & 0.182 & 0.019 & -0.017 \\ -0.01 & 0.019 & 0.186 & 0.032 \\ 0.011 & -0.017 & 0.032 & 1.643 \end{bmatrix}$$

The damping matrix (**C**) is estimated using the Rayleigh damping as Eq.(45).

$$\mathbf{C} = (\frac{2\xi\omega_i\omega_j}{\omega_i + \omega_j})\mathbf{M}^{Update} + (\frac{2\xi}{\omega_i + \omega_j})\mathbf{K}^{Update} \tag{45}$$

Here, ω_i, ω_j are the first and last available frequencies, respectively, and ξ the critical damping ratio has been obtained 0.2% from the experimental test.

3-2. Dynamic analysis using the Newmark method for harmonic loading

The unconditionally stable Newmark average acceleration method is recognized for its reliability, and the absence of numerical damping does not pose a significant challenge in its application [31]. This method is commonly employed to obtain the responses of structural systems. In this study, the effectiveness of the Newmark method within the direct integration framework was assessed through an analysis of a Single Degree of Freedom (SDF) system. A general damped SDF model was utilized to facilitate this evaluation, with its specifications detailed in Table 5.

Table 5- Parameters of a damped system (SDF)

m (kg)	k (kN/m)	ξ	$\bar{\omega}$ (rad/s)	p(t) (N)
3000	432	0.1% , 0.5%	1.2, 60	$-mg \sin(\bar{\omega}t)$

The analytical result of the SDF system for harmonic excitation is expressed as Eq.(46)

$$x(t) = \frac{p_0}{k} D \sin(\bar{\omega}t - \theta) + e^{-\xi\omega t}(A \cos\omega_D t + B \sin\omega_D t) \tag{46}$$

The values of the parameters in Eq.46) are calculated as Eq.(47)

$$D = \frac{1}{\sqrt{(1-\beta^2)^2 + (2\beta\xi)^2}}; \beta = \frac{\bar{\omega}}{\omega}; \theta = \tan^{-1}(\frac{2\beta\xi}{1-\beta^2}) \tag{47}$$

In Eq.(46), $\omega_D = \omega\sqrt{1-\xi^2}$ $p_0 = -mg$, and the initial conditions coefficients (A, B) are obtained in Eq.(48).

$$A = \frac{p_0}{k} D \sin\theta ; B = \frac{A\xi\omega - \frac{p_0}{k} D \bar{\omega}\cos\theta}{\omega_D} \tag{48}$$

In the context of harmonic excitation, the loading frequency was set at 12 rad/s, with a damping ratio (ξ) equal to 0.5%. The displacement response is illustrated in Figure 7. From a structural perspective, an excitation frequency equal to $\bar{\omega}$=12rad/s can be regarded as resonant in the context of a forced vibration problem. The figure indicates that the responses obtained through the Newmark method were greater than those derived analytically. This discrepancy is likely attributable to the effects of numerical damping and period elongation errors inherent in the Newmark method. Furthermore, Figure 7 demonstrates that under ordinary loading, the Newmark method performs adequately.
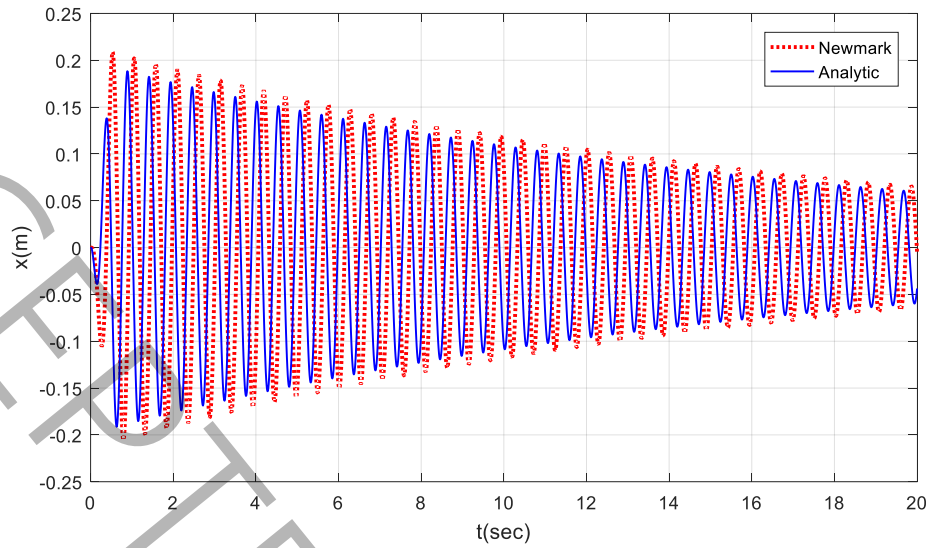
Fig.7- Displacement responses with the Newmark, HHT-alfa, and analytical methods for harmonic loading(

$\xi = 0.5\%$ and $\bar{\omega} = 12$ rad/s

3-3. Dynamic analysis under impact loading

The displacement results of the beam were analyzed to evaluate the efficacy of the Newmark method in the context of short-time loading. These results were compared with those obtained through the proposed analytical method and experimental testing. As illustrated in Figure 8, the beam was subjected to impulse loading at its free end on a laboratory scale. The measured accelerations at measurement stations CH1, CH2, CH3, and CH4 are depicted in Figure 8. The input and output data were utilized to validate the proposed analytical method and to demonstrate the capabilities of the Newmark method under impulse loading conditions.
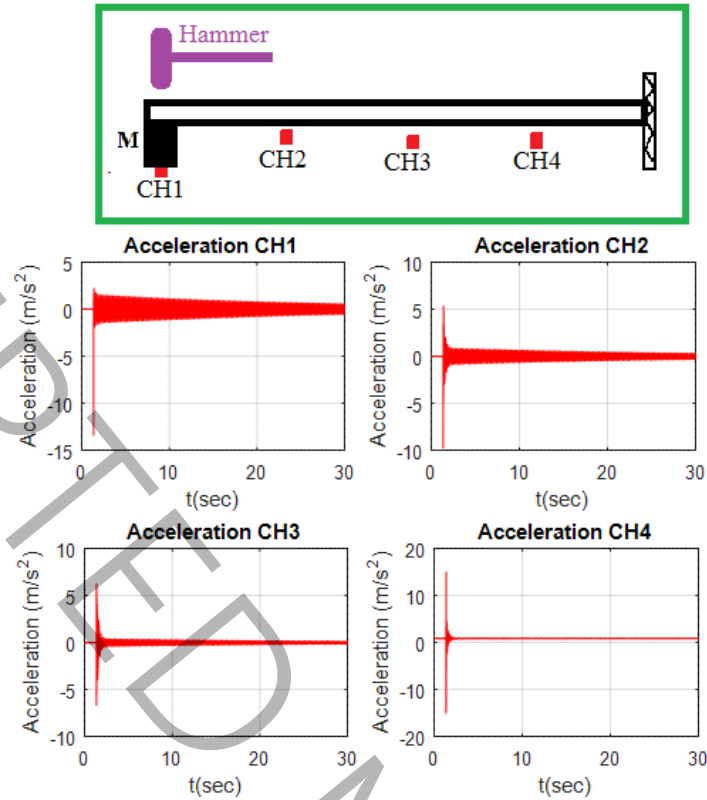
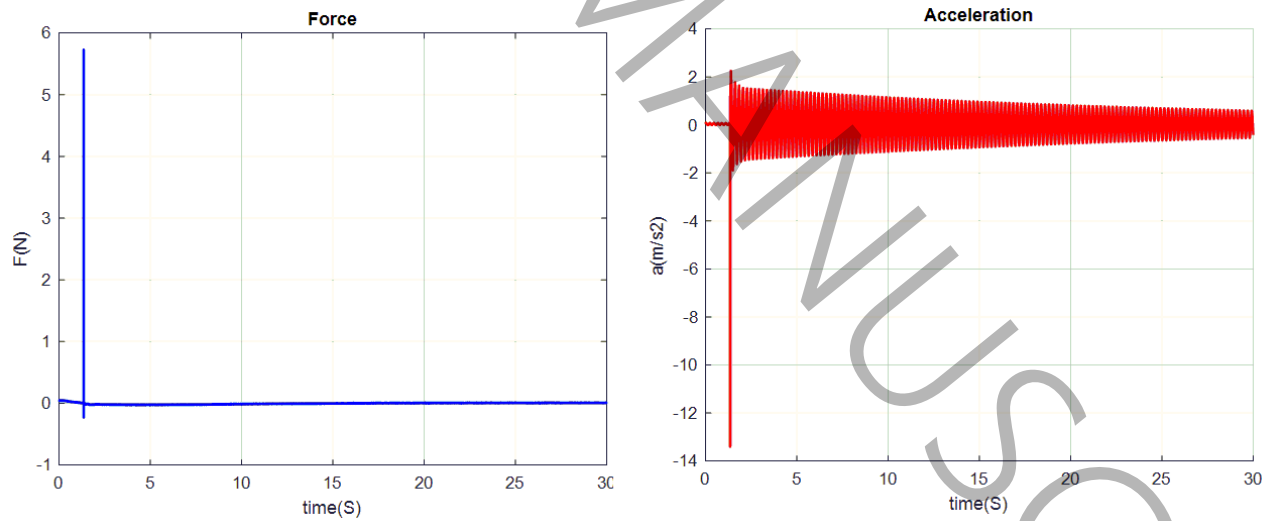Fig.8- Experimental accelerations at desired stations when the hammer is exerted at CH1

Fig.9- Applied load with a hammer CH1 station (left): Measured acceleration of the beam at CH1 (right)

The Newmark acceleration technique was employed to compute the numerical results for the beam, and these values were subsequently compared with the experimental data obtained at point CH1. As illustrated in Figure 10, there is a discrepancy between the experimental and numerical values, even after the finite element (FE) model was updated. Between 0 to 5 seconds, the numerical values are three times greater than the experimental ones. To the best of the authors' knowledge, the Newmark method is not suitable for shock-type loading, and the transient responses of low-

damping multi-degree-of-freedom (MDF) systems should be assessed using other techniques. This algorithm shares similarities with other numerical methods applied under short-time loadings and is associated with issues such as numerical damping, spurious frequency errors, period elongation, and amplitude decay errors.
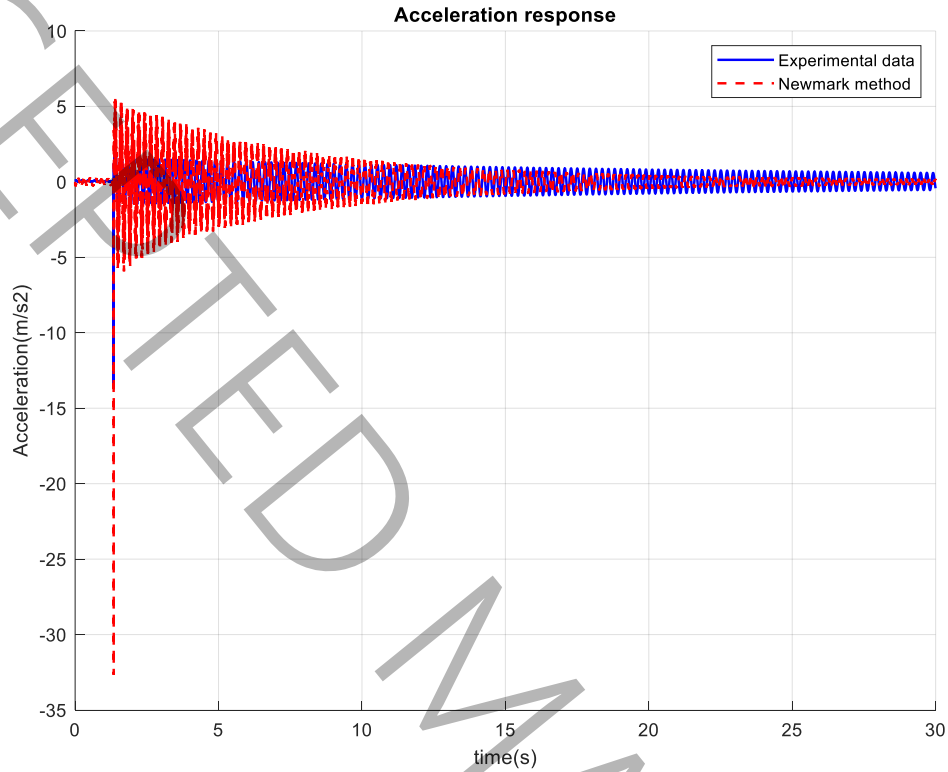

Fig.10- Acceleration of the beam (station CH1) using experimental data and the Newmark method

According to Figure 11, the response of the beam under this specific loading condition was evaluated using the proposed analytical method. As illustrated in Figure 11, the acceleration results from station CH1 are compared with those derived from the proposed analytical approach. Overall, the findings indicate a strong correlation between the proposed method and the experimental data. Notably, when the beam's free vibration commenced after 5.2 seconds, the amplitudes of the vibrations predicted by the proposed method did not exhibit any decay. This phenomenon can be attributed to the absence of internal or external damping in the partial differential equation governing the beam's behavior (as outlined in Eq. (19)), which results in the proposed analytical method being unable to account for damping effects. In contrast, the experimental response demonstrates a gradual reduction in the amplitude of free vibrations, attributable to small damping in the beam, which was determined to be approximately $\xi = 0.2\%$. This damping ratio was obtained through experimental testing conducted on the beam under investigation.
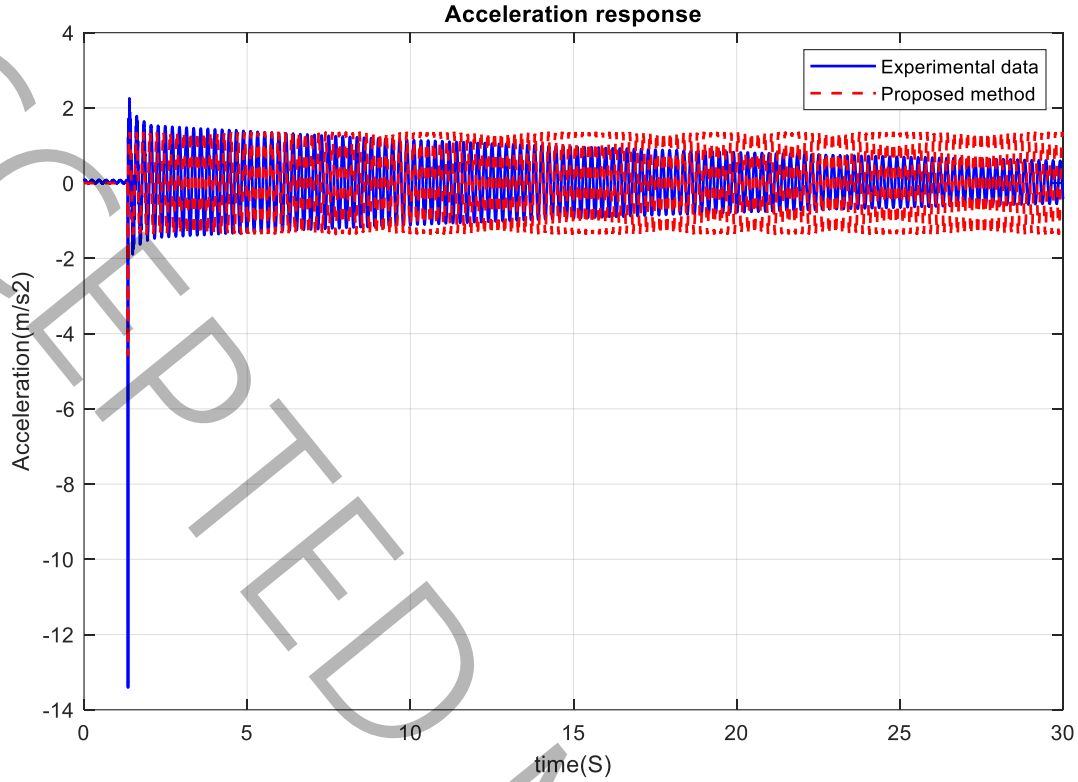
Fig.11- Acceleration at CH1 using the proposed analytical method and experimental data

4. Conclusions

This study investigates the dynamic behavior of an aluminum beam through the application of experimental, analytical, and numerical methods. An analytical formulation for the beam was derived as a main step. Subsequently, the finite element method was updated utilizing experimental modal data in conjunction with the particle swarm optimization technique. The derived analytical method and the updated finite element model were then employed to assess the beam's response under impulse loading conditions. The conclusions drawn from the results of this research are as follows:

• The Newmark HHT-alfa methods demonstrate remarkable numerical performance when applied to regular loadings, such as harmonic and earthquake excitations. However, the findings indicate that both the Newmark and HHT-alfa methods are inherently unconditionally stable, which limits their ability to accurately estimate structural responses under shock-type loading. Consequently, alternative methods should be employed for such loadings.

• The findings indicate that the proposed analytical method is capable of accurately estimating the responses of the MDF systems under very short-time loading conditions, without encountering issues such as numerical damping, period elongation, or amplitude decay errors.

- When the duration of the loading is very small, such as in cases of shock or impact loadings, the damping of the system may be ignored. Unlike the Newmark and HHT-alfa methods, the proposed analytical approach demonstrates insensitivity to this concern, thereby leading to reliable responses. Conversely, the Newmark and HHT-alpha techniques can not regulate numerical damping, resulting in numerical responses that significantly exceed actual values and are consequently overestimated.

- From a structural perspective, multi-degree-of-freedom (MDF) structures can be approximated as an equivalent single-degree-of-freedom (ESDF) system, albeit with certain modeling assumptions that may introduce errors. While formulations have been proposed specifically for the MDF system, the methodology presented applies to any MDF system that can be approximated by an equivalent SDF system (ESDF).

Conflict of interests

The authors declare that they have no conflicts of interest.

References

1. Tagarielli, V., V. Deshpande, and N. Fleck, Prediction of the dynamic response of composite sandwich beams under shock loading. International Journal of Impact Engineering, 2010. 37(7): p. 854–864.
2. Wan, H.-P. and W.-X. Ren, A residual-based Gaussian process model framework for finite element model updating. Computers & Structures, 2015. 156: p. 149–159.
3. Mazurkiewicz, Ł., et al., Comparison of numerical testing methods in terms of impulse loading applied to structural elements. Journal of Theoretical and Applied Mechanics, 2013. 51(3): p. 615–625.
4. Zhang, X., H. Hao, and Z. Wang, Experimental study of laminated glass window responses under impulsive and blast loading. International Journal of Impact Engineering, 2015. 78: p. 1–19.
5. Mohammad, R., A. Kotousov, and J. Codrington, Analytical modelling of a pipe with flowing medium subjected to an impulse load. International journal of impact engineering, 2011. 38(2-3): p. 115–122.
6. Stoynova, I. and T. Christov. Response of a reinforced concrete cantilever beam subject to impulse impact loads. in IOP Conference Series: Materials Science and Engineering. 2020. IOP Publishing.
7. Børvik, T., et al., Response of structures to planar blast loads–A finite element engineering approach. Computers & Structures, 2009. 87(9-10): p. 507–520.
8. Shiuh-Chuan, H. and L. Ching-Chun, Elastic responses of a composite shell structure subjected to impact loading. Materials Science, 2022. 28(1): p. 53–59.
9. Pradhan, S. and S. Modak, Normal response function method for mass and stiffness matrix updating using complex FRFs. Mechanical Systems and Signal Processing, 2012. 32: p. 232–250.
10. Arora, V., S. Singh, and T. Kundra, Comparative study of damped FE model updating methods. Mechanical Systems and Signal Processing, 2009. 23(7): p. 2113–2129.

11. Arora, V., S. Singh, and T. Kundra, Finite element model updating with damping identification. Journal of Sound and Vibration, 2009. 324(3-5): p. 1111–1123.
12. Yuan, Y., A model updating method for undamped structural systems. Journal of computational and applied mathematics, 2008. 219(1): p. 294–301.
13. García-Palencia, A.J. and E. Santini-Bell, A two-step model updating algorithm for parameter identification of linear elastic damped structures. Computer-Aided Civil and Infrastructure Engineering, 2013. 28(7): p. 509–521.
14. Esfandiari, A., et al., Structural model updating using frequency response function and quasi-linear sensitivity equation. Journal of sound and vibration, 2009. 326(3-5): p. 557–573.
15. Esfandiari, A., et al., Structural finite element model updating using transfer function data. Computers & structures, 2010. 88(1-2): p. 54–64.
16. Sipple, J.D. and M. Sanayei, Finite element model updating using frequency response functions and numerical sensitivities. Structural Control and Health Monitoring, 2014. 21(5): p. 784–802.
17. Li, W.-M. and J.-Z. Hong, New iterative method for model updating based on model reduction. Mechanical Systems and Signal Processing, 2011. 25(1): p. 180–192.
18. Weng, S., et al., Inverse substructure method for model updating of structures. Journal of Sound and Vibration, 2012. 331(25): p. 5449–5468.
19. Papadimitriou, C. and D.-C. Papadioti, Component mode synthesis techniques for finite element model updating. Computers & structures, 2013. 126: p. 15–28.
20. Sarmadi, H., A. Karamodin, and A. Entezami, A new iterative model updating technique based on least squares minimal residual method using measured modal data. Applied mathematical modelling, 2016. 40(23-24): p. 10323–10341.
21. Wei, S., et al., Modal identification of multi-degree-of-freedom structures based on intrinsic chirp component decomposition method. Applied Mathematics and Mechanics, 2019. 40(12): p. 1741–1758.
22. Christodoulou, K., et al., Structural model updating and prediction variability using Pareto optimal models. Computer Methods in Applied Mechanics and Engineering, 2008. 198(1): p. 138–149.
23. Jung, D.-S. and C.-Y. Kim, Finite element model updating on small-scale bridge model using the hybrid genetic algorithm. Structure and Infrastructure engineering, 2013. 9(5): p. 481–495.
24. Shabbir, F. and P. Omenzetter, Particle swarm optimization with sequential niche technique for dynamic finite element model updating. Computer-Aided Civil and Infrastructure Engineering, 2015. 30(5): p. 359–375.
25. Akbari, J., L. Nazari, and S. Mirzaei, Vibration Response Evaluation under Shock-Type Loading with Emphasis on Finite Element Model Updating. Shock and Vibration, 2020. 2020(1): p. 8861827.
26. Gilat, A., Numerical Methods for Engineers and Scientists.
27. Xie, W.-C., Differential equations for engineers. 2010: Cambridge university press.
28. Xue, D. and Y. Chen, Scientific computing with MATLAB. 2018: Chapman and Hall/CRC.
29. Friswell, M.I. and J. Mottershead, Finite element model updating in structural dynamics. 1995: Kluwer Academic Publishers.
30. Erdogmus, P., Particle swarm optimization with applications. 2018: BoD–Books on Demand.
31. Paultre, P., Dynamics of structures. 2013: John Wiley & Sons.